Structure, Magnetic Properties and Magnetization Reversal Processes in Nanocrystalline $Pr_8Dy_1Fe_{60}Co_7Mn_6B_{14}Zr_1Ti_3$ Bulk Alloy

ANNA PRZYBYL*, IZABELA WNUK, JERZY J. WYSLOCKI
Institute of Physics, Czestochowa University of Technology, Armii Krajowej 19 Av., 42-200 Czestochowa, Poland

The present paper presents results concerning on structure, magnetic properties and magnetization reversal processes in the as-cast $Pr_8Dy_1Fe_{60}Co_7Mn_6B_{14}Zr_1Ti_3$ alloy in the form of 1 mm plate. The XRD studies revealed coexistence of three phases dominant $Pr_2(Fe,Co)_{14}B$ and minor á-Fe and Fe_3B. The remanence-to-saturation ratio J_r/J_s equaled 0.66 and indicated on existence of strong exchange interactions between hard and soft magnetic phases. The analysis of M_{rev} vs. M_{irr} dependences, the pinning mechanism was detected in studied alloy.

Keywords: bulk alloys, magnetic properties, magnetization reversal processes

Since over than 30 years, the $RE_2Fe_{14}B$- type alloys (where RE= Pr, Nd, Dy or Tb) have been intensively studied due to their excellent magnetic properties. This type of alloys are used as permanent magnets in motors, as record heads, wind energy turbines and miniaturized electronic devices [1,2]. Nanocrystalline composites based on $RE_2Fe_{14}B$/á-Fe exhibit interaction between soft magnetic á-Fe phase and hard magnetic $RE_2Fe_{14}B$ or pinning of domain walls, which results in higher saturation magnetization compared to single phase material based on $RE_2Fe_{14}B$ phase [3,4]. Recently, an intensively studies concerning on replacing Nd or Pr by La, Ce and Y have been carried out [5-17] in order to reduce critical elements like Nd, Pr or Dy. In previous paper, the magnetic properties of melt-spun $Pr_8Dy_1Fe_{60}Co_7Ni_{6-x}Mn_xB_{14}Zr_1Ti_3$ were investigated. An enhancement of remanence and square hysteresis loops were revealed [18]. Moreover, detailed studies shown that the presence of Ni causes an increase of remanence, while Mn results in rise of coercivity. Further studies concerned on magnetization reversal processes in bulk alloys with the same composition [19]. In investigated alloys in form of tubes, the mechanism of magnetization reversal based on nucleation and pinning processes. Due to the fact that internal structure and properties of material prepared by various techniques could be different, we decided to study phase composition, magnetic properties and magnetization reversal processes in 1mm plate of the $Pr_8Dy_1Fe_{60}Co_7Mn_6B_{14}Zr_1Ti_3$ and it was the main aim of following paper.

Experimental part

The ingot sample, corresponding to chemical composition $Pr_8Dy_1Fe_{60}Co_7Mn_6B_{14}Zr_1Ti_3$, was obtained by arc melting of high purity of constituent elements under low pressure of Ar. Sample was remelted ten times in order to homogeneity of material. Then, sample in form 1mm plate was produced by suction casting technique under Ar atmosphere. The phase composition of the sample was investigated using Bruker D8 Advance diffractometer equipped with Cu X-ray tube and superconducting LynxEye detector. The X-ray diffraction was supported by the Rietveld analysis using PowderCell package [20]. The broadening of the diffraction reflexions allowed to calculate the average grain size for recognized phased using Scherrer's method. The room temperature major, minor hysteresis loops and sets of recoil curves were measured using LakeShore VSM 7307 in external magnetic field up to ~2T. Magnetization reversal processes were studied using reversal recoil curves.

Results and discussions

The XRD pattern of the $Pr_8Dy_1Fe_{60}Co_7Mn_6B_{14}Zr_1Ti_3$ sample was depicted in Fig.1. The Rietveld analysis revealed coexistence of three different crystalline phases: $Pr_2(Fe,Co)_{14}B$ (82 vol.%), α-Fe (5 vol. %) and Fe_3B (13 vol. %). The obtained phase structure is expected due to potential application material as a permanent magnet. Estimated average grain size using Scherrer's equation for the studied sample are 10 nm, 18 nm and 11 nm, for α-Fe, $Pr_2(Fe,Co)_{14}B$ and Fe_3B phase, respectively.

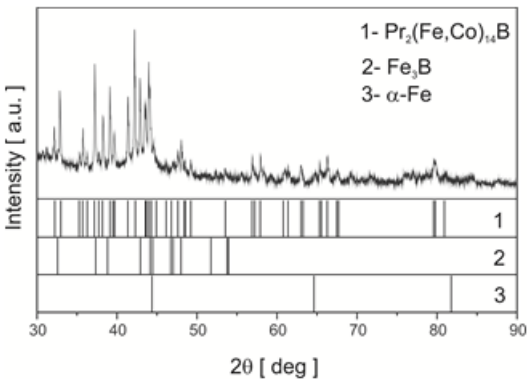

Fig. 1. XRD scans measured for the as-cast $Pr_8Dy_1Fe_{60}Co_7Mn_6B_{14}Zr_1Ti_3$ alloy in the form of 1 mm plate.

Measured hysteresis loop is shown in Fig. 2. The hysteresis loop is typical for single phase material. Moreover, the shape virgin curve is characteristic for materials for which the main magnetization reversal mechanism is a pinning of domain walls. The remanence-to-saturation ratio J_r/J_s equals 0.66 and confirms the existence of strong exchange interactions between hard and soft magnetic phases revealed in produced material. The magnetic parameters of the as-cast $Pr_8Dy_1Fe_{60}Co_7Mn_6B_{14}Zr_1Ti_3$ alloy in the form of 1 mm plate are summarized in Tab. 1.

The magnetization reversal processes in the $Pr_8Dy_1Fe_{60}Co_7Mn_6B_{14}Zr_1Ti_3$ alloy 1mm plate were studied using measured recoil curves (Fig. 3). Based on these curves, the dependences of reversible parts M_{rev} on the irreversible parts M_{irr} of magnetization for external magnetic field changes were constructed and are plotted in Fig. 4.

* email: przybyl.anna@wip.pcz.pl

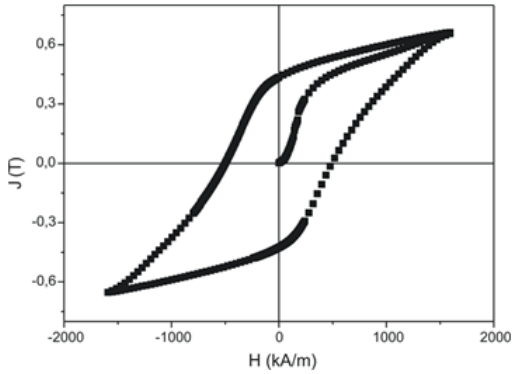

Fig. 2. The hysteresis loops and initial magnetization curves measured for the $Pr_8Dy_1Fe_{60}Co_7Mn_6B_{14}Zr_1Ti_3$ alloy 1mm plate

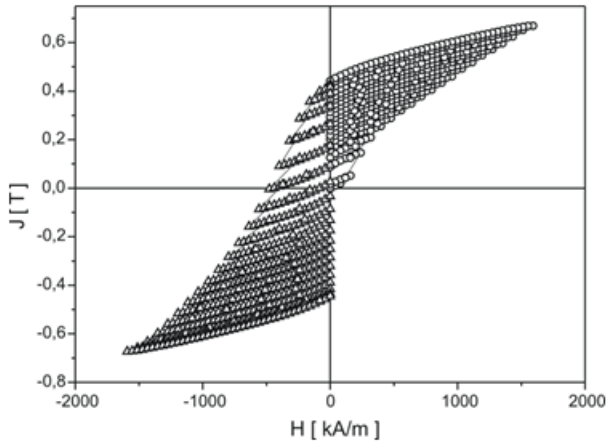

Fig. 3. Magnetization recoil curves measured for the initially saturated nanocrystalline $Pr_8Dy_1Fe_{60}Co_7Mn_6B_{14}Zr_1Ti_3$ alloy 1mm plate

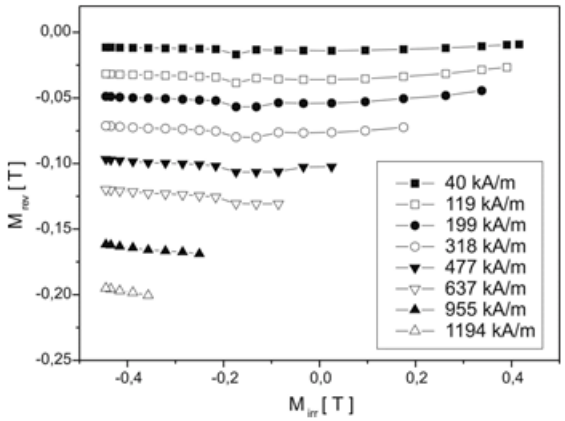

Fig. 4. Plots of reversible part of magnetization M_{rev} as a function of irreversible magnetization M_{irr} for the $Pr_8Dy_1Fe_{60}Co_7Mn_6B_{14}Zr_1Ti_3$ alloy 1mm plate.

The dominant magnetization reversal process of the sample can be determined based on shape of M_{rev} vs. M_{irr} dependences. The nucleation process is dominant for permanent magnets, where reversed domains once nucleated and then expand through the grains. In Fig. 4, the almost straight lines with negative slope are visible. For materials with pinning of domain walls, the minimum in the M_{rev} vs. M_{irr} curves is observed. Slight minimum is visible in Fig. 4, which confirms the presence of pinning mechanism in the studied sample. This shape of presented curve indicates that reversal magnetization process is a mixture between nucleation and pinning.

In order to further clarify the coercivity mechanism and the occurrence of possible interactions, remanence curves and Henkel plots were determined. To demonstrate the exchange-coupling the calculation of δM plots (δM(H))

Table 1

COERCIVITY $_JHc$, REMANENCE POLARIZATION J_r, SATURATION POLARIZATION J_s, MAXIMUM ENERGY PRODUCT $(BH)_{max}$ And THE REMANENCE-TO-SATURATION RATIO J_R/J_s MEASURED FOR THE $Pr_8Dy_1Fe_{60}Co_7Mn_6B_{14}Zr_1Ti_3$ ALLOY 1mm PLATE

	$_JHc$ [kA/m]	J_r [T]	J_s [T]	$(BH)_{max}$ [kJ/m^3]	J_r/J_s
$Pr_8Dy_1Fe_{60}Co_7Mn_6B_{14}Zr_1Ti_3$	495	0.43	0.66	29	0,66

[21] were carried out using formula $\delta M = m_d(H) - [1 - 2m_r(H)]$, were $m_d(H)$ is reduced demagnetization remanent magnetization (DCD) acquired after saturation in one direction and then the subsequent application and removal of a direct field H in the reverse direction and $m_r(H)$ is the reduced isothermal remanence (IRM) acquired after the application and subsequent removal of a field H. The two remanence curves of IRM and DCD measured for the $Pr_8Dy_1Fe_{60}Co_7Mn_6B_{14}Zr_1Ti_3$ alloy 1mm plate are shown in Fig. 5.

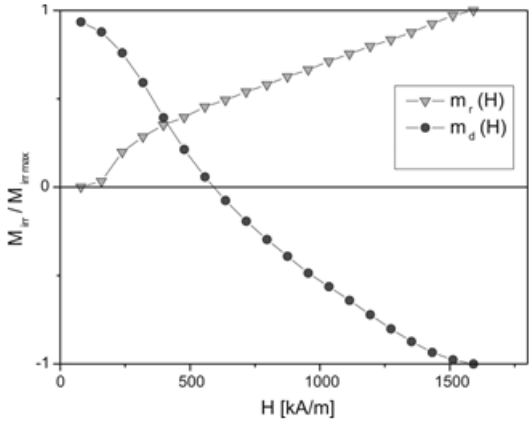

Fig.5. Normalized field dependence of the IRM ($m_r(H)$) and DCD ($m_d(H)$) remanence curves determained for the $Pr_8Dy_1Fe_{60}Co_7Mn_6B_{14}Zr_1Ti_3$ alloy 1mm plate.

These curves can provide information about the irreversible distribution of the energy barrier, while the differentiation of these relationships allows to determine the contribution of both the nucleation of new domains and the pinning domain walls in the magnetization reversal process. The domain wall pinning energy distribution can be determined by the differentiation of the IRM curve while DCD curve differentiation determines both domain wall pinning and nucleation energy distribution. Fig 6 shows the differentiation curves of the IRM and DCD remanence (SFD) calculated for the $Pr_8Dy_1Fe_{60}Co_7Mn_6B_{14}Zr_1Ti_3$ alloy 1mm plate.

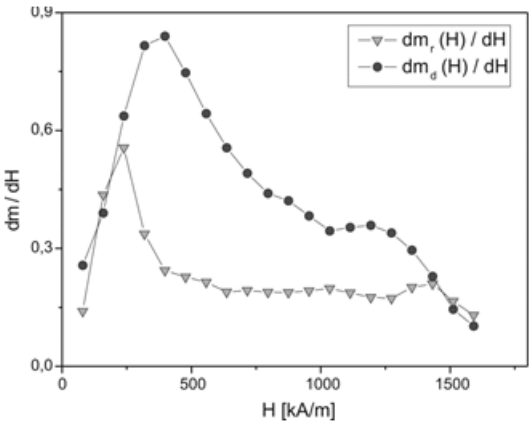

Fig. 6. Switching field distribution (SFD) of the $Pr_8Dy_1Fe_{60}Co_7Mn_6B_{14}Zr_1Ti_3$ alloy 1mm plate.

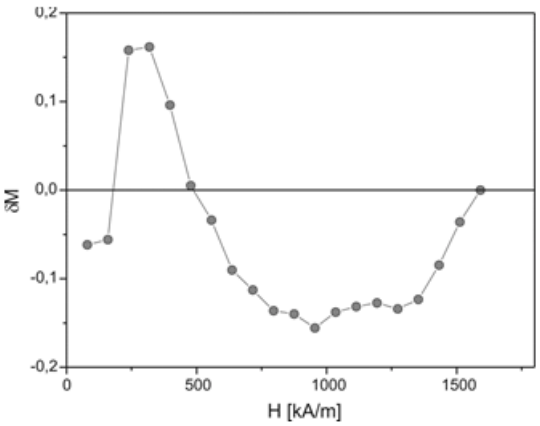

Fig.7. Henkel plots of the $Pr_8Dy_1Fe_{60}Co_7Mn_6B_{14}Zr_1Ti_3$ alloy 1mm plate.

On the IRM differential curve a single, fairly sharp peak can be observed in the area of low magnetic fields (~ 250 kA/m) and a wide tail extending towards high magnetic fields. On the other hand, the DCD differential curve shows a much higher peak slightly shifted to the right (around the ~400 kA/m magnetic field) and another much smaller peak in the high field. The results indicate that weak domain wall pinning firstly, and then both nucleation and pinning effect occur and the coercivity is mainly determined by reversal domain nucleation.

In Figure 7 the δM plots for the $Pr_8Dy_1Fe_{60}Co_7Mn_6B_{14}Zr_1Ti_3$ alloy 1mm plate is presented. The positive value of δM indicates an exchange interaction between magnetic moments. The negative value δM indicates a magnetostatic interaction, and isolated single domain grains or non-interacting grains show a value of zero. In present research initially, in low magnetic fields up to about 200 kA/m, the δM curve takes negative values, which indicates the magnetostatic interactions are dominant. The strongest intergranular exchange-coupling interactions, related to positive δM values, present in range of magnetic field from 200 to 500 kA/m, are observed. It can be seen that trend for the plot is for δM to increase to a peak, then decrease rapidly around the coercivity. δM reaches a negative minimum and then starts to increase again. The study of coercivity mechanism and the possible interactions is very important for further guidance increase its value and to develop high performance nanocomposite magnets.

Conclusions

We have show that the nanocrystalline permanent magnets based on $(Pr,Dy)_2(Fe,Co,Mn)_{14}B$ phase could produced from amorphous phase. The XRD studies revealed coexistence of the hard magnetic $(Pr,Dy)_2(Fe,Co,Mn)_{14}B$ phase with soft magnetic α-Fe and Fe_3B phases. The Rietveld analysis shown that the dominant phase is the $(Pr,Dy)_2(Fe,Co,Mn)_{14}B$. The magnetic studies allowed to conclude that in produced sample, strong coupling interactions are observed. The studies of reversal magnetization processes suggest an occurrence of combined magnetization reversal process (nucleation and pinning) in investigated sample.

References

1.REHMAN, S.U., JIANG, Q., HE, L., GHAZANFAR, M., LEI, W., HU, X., AWAN, S.U., MA, S., ZHONG, Z.C., J. Magn. Magn. Mater. **466,** 2018, p.377.
2.GUTFLEISCH, O., WILLARD, M.A., BRÜCK, E., CHEN, C.H., SANKAR, S.G., LIU, J.P., Adv. Mater. **23** no.7, 2011, p.821.
3.SCHREFL, T., FISCHER, R., FIDLER, J., KRONMÜLLER, H., J. Appl. Phys. **76,** 1994, p.7053.
4.SHANDONG, L., GU, B.X., SEN, Y., HONG, B., YAODONG, D., ZONGJUN, T., GUOZHI, X., YOUWE, D., ZUANRU, Y., J. Phys. D: Appl. Phys. **35**, 2002, p.732.
5.LIAO, X.F., ZHANG, J.S., YU, H.Y., ZHONG, X., KHAN, A.J., ZHOU, X., ZHANG, H., LIU, Z.W., J. Mater. Sci., 2019, DOI: https://doi.org/10.1007/s10853-019-03916-8.
6.HUSSAIN, M., ZHAO, L.Z., AKRAM, R., AHMAD, Z., ZHANG, Z.Y., GULZAR, A., ZHONG, X.C., LIU, Z.W., J. Magn. Magn. Mater. **468**, 2018, p.141.
7.LIAO, X.F., ZHANG, J.S., YU, H.Y., ZHONG, X., LIU, Y., LIU, Y.T., LIU, Z.W., J. Magn. Magn. Mater. **489,** 2019, p.165444.
8.NABIALEK, M., BLOCH, K., SZOTA, M., SANDU, A.V., Mat. Plast., **54**, no. 3, 2017, p. 491.
9.BLOCH, K., TITU, M.A., SANDU, A.V., Rev.Chim. (Bucharest), **68**, no. 9, 2017, p. 2162.
10.PAPADATU, C.P., SANDU, A.V., BORDEI, M., SANDU, I.G., Rev.Chim. (Bucharest), **68**, no. 4, 2017, p. 675.
11.GRUSZKA, K., NABIALEK, M., SZOTA, M., VIZUREANU, P., ABDULLAH, M.M.A., BLOCH, K., SANDU, A.V., Rev.Chim. (Bucharest), **68**, no. 2, 2017, p. 265.
12.POIANA, M., DOBROMIR, M., SANDU, A.V., GEORGESCU, V., Journal Of Superconductivity And Novel Magnetism, **25**, 7, 2012, p. 2377.
13.TOMA, S.L., BEJINARIU, C., GHEORGHIU, D.A., BACIU, C., Advanced Materials Research, 814, 2013, p. 173.
14.BACAITA, E.S., BEJINARIU, C., ZOLTAN, B., PEPTU, C., ANDREI, G., POPA, M., MAGOP, D., AGOP, M., Journal Of Applied Mathematics, 2012, Article Number: 653720
15.ACHITEI, D.C., VIZUREANU, P., DANA, D., CIMPOESU, N., Metalurgia International, **18**, SI2, 2013, p. 104.
16.BALTATU, S., VIZUREANU, P., MARECI, D., BURTAN, L.C., CHIRUTA, C., TRINCA, L.C., Materials And Corrosion-Werkstoffe und Korrosion, **67**, 12, 2016, p. 1314.
17.TANASE, S.I., TANASE, D., PASCARIU, P., VLAD, L., SANDU, A.V., GEORGESCU, V., Materials Science And Engineering B, **167,** 2010, p. 119.
18.PRZYBYL, A., PAWLIK, K., PAWLIK, P., GEBARA, P., WYS£OCKI, J.J., J. All. Compd. **536S,** 2012, p.S333.
19.PRZYBYL, A., PAWLIK, K., PAWLIK, P., GEBARA, P., WYS£OCKI, J.J., Acta Phys. Pol. **A 127**, 2015, p.579.
20.KRAUTZ, W., NOLZE, G., Powder Diffr. **13**, 1998, p.256.
21.KELLY, P.E., O'GRADY, K., MAYO, P.I., CHANTRELL, R.W., IEEE Trans. Magn. **25,** 1989, p.3881.

Manuscript received: 12.11.2018